Spatially averaged model of complex-plasma discharge with self-consistent electron energy distribution

I. Denysenko* and M. Y. Yu†
Theoretical Physics I, Ruhr University, D-44780 Bochum, Germany

K. Ostrikov‡
School of Physics, The University of Sydney, Sydney, NSW 2006, Australia

A. Smolyakov
Department of Physics and Engineering Physics, University of Saskatchewan, Saskatoon, Saskatchewan, Canada S7N 5E2
(Received 27 December 2003; revised manuscript received 18 June 2004; published 7 October 2004)

A global, or averaged, model for complex low-pressure argon discharge plasmas containing dust grains is presented. The model consists of particle and power balance equations taking into account power loss on the dust grains and the discharge wall. The electron energy distribution is determined by a Boltzmann equation. The effects of the dust and the external conditions, such as the input power and neutral gas pressure, on the electron energy distribution, the electron temperature, the electron and ion number densities, and the dust charge are investigated. It is found that the dust subsystem can strongly affect the stationary state of the discharge by dynamically modifying the electron energy distribution, the electron temperature, the creation and loss of the plasma particles, as well as the power deposition. In particular, the power loss to the dust grains can take up a significant portion of the input power, often even exceeding the loss to the wall.

DOI: 10.1103/PhysRevE.70.046403 PACS number(s): 52.25.Vy, 52.27.Lw, 52.77.Dq, 52.80.Pi

I. INTRODUCTION

Low-pressure plasmas are widely used in the semiconductor, optical, and other modern industries for the fabrication of microelectronic, optoelectronic, and photonic devices, for plasma enhanced chemical vapor deposition (PECVD) of multilayered functional coatings, etc., as well as for environmental remediation [1–4] and nanostructured materials manufacturing [1,5]. The plasmas are complex multicomponent systems containing electrons, ions, neutrals, and charged "dust" grains of much larger size, charge, and mass. The dust grains can be either desired working material or unwanted pollutants. They are usually produced by plasma-surface interaction or by clustering and agglomeration of molecules generated by chemical reactions within the plasma [1]. The grains are typically tens of nm to tens of μm in size and their density can be as high as 10^8 cm^{-3} in low-pressure rf plasmas, and they are usually in a colloidal state within the plasma.

Plasma-grown nanoclusters and fine powder particles can dramatically affect the discharge characteristics and the deposition process. Existing results show a direct link between the density and charge of the dust grains, as well as the electron temperature of the bulk plasma, to the quality of the PECVD fabricated films [1,6–11]. For example, in the PECVD of amorphous silicon, device-grade films can be produced under low grain density and low electron temperature conditions [12]. Growth, but without agglomeration, of clusters and crystallites is also often desired [7–9,13]. On the other hand, self-organization of nanoclusters and nanoparticles into ordered or disordered building blocks is crucial for the fabrication of exotic objects, such as the cluster-assembled carbon nanofoam with unusual semiconducting and ferromagnetic properties [14]. Thus, efficient management of the grain size and density [15] is crucial in plasma-assisted deposition of advanced nano-materials and biomaterials [13,16–18]. Recently, the evolution and stationary states of dusty plasma systems have been investigated. These include the dust transport and stability phenomena [19–21] as well as dust origin and growth [1,22–24].

Existing theoretical approaches to dusty plasma discharges are mostly limited to relatively low ion density ($n_i \leqslant 10^9$ cm^{-3}) rf capacitively coupled plasmas (CCPs) that have been widely used in the semiconductor industry and in the laboratory. Recently, for industrial use the CCPs have gradually been replaced by the higher density inductively coupled plasmas (ICPs) [25,26] and microwave plasmas [27]. These plasmas are characterized by higher densities ($n_i \gtrsim 10^{10}$ cm^{-3} in the high density discharges) and lower sheath potentials than that of CCPs. Methods for dust control developed for CCPs [1] are often not applicable to ICPs and microwave plasmas. In fact, the physics of high-density dusty plasmas is still not well understood.

For analysis of pristine (dust-free) ICPs, fluid [28–30], local and nonlocal kinetic approaches [31,32], as well as particle-in-cell (PIC) simulation [33,34], have been used. Spatially averaged, or global, models have been shown to be useful in understanding ICPs [35]. Such global models allow one to obtain plasma parameters averaged over the bulk vol-

*Permanent address: School of Physics and Technology, Kharkiv National University, 61077 Kharkiv, Ukraine.
†Corresponding author. Email address: yu@tp1.rub.de
‡Also at Plasma Sources and Applications Center, NIE, Nanyang Technological University, 637616 Singapore.

ume of the plasma, and analyze the energy loss in particle collisions as well as to the walls. They are much simpler than the more elaborate local models and simulations [36] and thus do not require much computational resource. Nevertheless, the key plasma parameters can be deduced from the relatively simple conservation equations of the global models [35].

In this paper we present a self-consistent global model for argon discharges containing dust grains. The model consists of particle and power balance equations for the averaged electron and ion densities, electron temperature, and power loss in the discharge. In contrast to most earlier models of dust-containing discharges [1,2,22,23,37], power loss to the dust grains is also included. The average dust charge is calculated using the conventional orbit motion limited (OML) approach. In existing global models the electron energy distribution function (EDF) is usually assumed to be Maxwellian. However, the electrons are very often far from equilibrium. Here, we generalize our earlier model for complex plasma discharge [2,15,19,20,37] by self-consistently solving for the EDF from the electron Boltzmann equation.

Accordingly, we shall solve the particle and power balance equations, the electron Boltzmann equation including the major sources and sinks, together with the boundary conditions for the ICP. Our aim is to investigate the effects of the dust grains and external discharge parameters, such as the input power and operating pressure, on the discharge characteristics, such as the EDF, the electron and ion densities, the dust charge, etc. Power loss in the complex plasma system is included in detail. The calculations are carried out for discharge conditions typical of laboratory ICPs and microwave plasmas. Thus, our results can be used to improve the design and management of the deposition processes. Because of the simplicity of the model, the computation time is much shorter. The present global model is thus especially useful for online diagnostics and feedback control of the discharge itself as well as of the processing.

II. THEORETICAL MODEL

A. Main assumptions

We consider an rf or microwave low-pressure argon discharge of radius R and of length L containing dust grains. The discharge is maintained by an electric field $E(t) \sim \exp(i\omega t)$, where $\omega = 2\pi f_E$. The frequencies $f_E = 13.56$ MHz and $f_E = 2.45$ GHz shall be considered. The plasma is composed of electrons, singly charged positive ions Ar^+, and negatively charged colloidal dust grains. We assume that the dust grains are all of the same size and are uniformly distributed in the plasma column, except in a dust-free boundary layer of thickness l near the wall. This profile of the dust density is typical in dust-growth experiments using argon-silane mixtures [38] and appears when the dust grains are created in the silane-argon mixture and trapped in the argon discharge [39]. We also assume that $\tau_d \gg \tau_{eq}$, where τ_d and τ_{eq} are the characteristic time scales of dust grain motion and establishment of equilibrium, respectively. Therefore, the massive dust grains can be treated as immobile. It is also assumed that $\lambda_D \gg a_d$ and $d \gg \lambda_D$, where λ_D is the Debye length, a_d the dust grain radius, $d = n_d^{-1/3}$ the distance between the dust grains, and n_d the dust density.

The dust shielding potential is given by [1]

$$\phi(r) = \phi_s \frac{a_d}{r} \exp\left(- \frac{r - a_d}{\lambda_D} \right), \tag{1}$$

where $\lambda_D^{-2} = 4\pi e (n_e / T_e + n_i / 2E_0)$, ϕ_s is the dust surface potential, n_i the ion density in the dusty region, E_0 (=0.06 eV) and T_e the average ion energy and electron temperature (in eV), and e the elementary charge. Daugherty *et al.* [40] showed that except for very large dust grains, Eq. (1) is very close to that from the numerical solutions of the corresponding nonlinear Debye-Hückel theory, and that it is a good approximation for $a_d \leqslant 1$ μm. Kennedy and Allen [41] recently studied the electrostatic potential around a small ($a_d / \lambda_{De} \sim 10^{-3}$, where λ_{De} is the electron Debye length) dust grain using a generalized OML theory. They found that noticeable deviation from Eq. (1) appears only at large distances from the grain.

B. Electron kinetic equation

In an electric field $\mathbf{E}$, the electron velocity distribution function $f(\mathbf{r}, \mathbf{v}, t)$, where $\mathbf{r}$ and $\mathbf{v}$ are coordinate and velocity of the electrons and t is the time, satisfies the well-known Boltzmann equation [42,43]

$$\frac{\partial f}{\partial t} + \nabla_r \cdot (\mathbf{v} f) - \nabla_v \cdot \left(\frac{e\mathbf{E}}{m_e} f \right) = \left(\frac{\delta f}{\delta t} \right)_c, \tag{2}$$

where $(\delta f / \delta t)_c$ is the time rate of change f due to collisions, and m_e is the electron mass. The electron density n_e is given by $n_e(\mathbf{r}, t) = \int f d^3 v$. The total electric field $\mathbf{E} = \mathbf{E}_s + \mathbf{E}_p \exp(i\omega t)$ consists of a space-charge field E_s and an external RF field E_p at frequency ω.

Traditionally, for systems not too far from equilibrium, Eq. (2) is solved by expanding the EDF in spherical harmonics together with Fourier analysis in time [42,43]. That is, one writes

$$f = \sum_l \sum_p F_p^l P_l(\cos\theta) \exp(ip\omega t), \tag{3}$$

where P_l is the Legendre polynomial of order l and θ is the polar angle. Neglecting terms beyond the first order (i.e., in the Lorentz approximation), we have $f(\mathbf{r}, \mathbf{v}, t) = f_0(\mathbf{r}, v, t) + (\mathbf{v}/v) \cdot \mathbf{f}_1(\mathbf{r}, v, t)$, where the isotropic part f_0 describes the energy distribution of random motion, while the anisotropic part f_1 describes the directed motion in the electric field. The Lorentz approximation is valid when there is sufficiently large number of elastic collisions [44], so that the distribution is almost isotropic ($f_0 \gg f_1$). It is valid for electrons in the elastic (energies below the excitation thresholds) as well as inelastic (energies above the excitation thresholds) regimes [31], and is widely used for studying low-pressure discharges and collisional plasmas in general (see, e.g., Refs. [31,32] and the references therein). The EDFs of the low-energy electrons are usually isotropic, provided that the discharge dimension is larger than the electron mean free path. On the other hand, due to a large difference in the cross

sections of elastic and inelastic collisions and the much smaller number density of the high-energy electrons, electron momentum relaxation occurs much faster than that of energy, so that the EDF in the high-energy inelastic-collision regime is also nearly isotropic [31,32].

We also assume that f_0 is time independent, which is valid if [45,46]

$$\omega > \nu_e = (2m_e/m_i)\nu_m + \nu^*, \tag{4}$$

where ν^* is the total inelastic collision frequency, m_i is the ion mass, and ν_m is the collision frequency for momentum transfer. The field variation in most stable discharges is usually much faster than that of energy relaxation, so that their temporal effects average out in the isotropic part of the EDF and the condition (4) is satisfied.

When the plasma size and neutral pressure are sufficiently high, the inequality $p_0 L > 100$ m Torr cm [44], where p_0 is neutral pressure in mTorr and L is the size of the discharge in cm, has to be satisfied. Furthermore, when the electron density is sufficiently high ($\lambda_{De} \ll L$, such as in quasineutral discharges), the spatial derivative term in Eq. (2) and the space-charge electric field $\mathbf{E}_s$ can be safely neglected [47]. It is then convenient to separate the variables and rewrite $f_0(\mathbf{r},v)$ as

$$f_0 = n_e(\mathbf{r})F(v), \tag{5}$$

where $\int_0^\infty F(v)4\pi v^2\, dv = 1$, and to change the variable from velocity to energy ($\varepsilon = m_e v^2/2e$). Accordingly, we introduce the electron energy distribution $F_0(\varepsilon)$ by the relation $F(v)4\pi v^2\, dv = F_0(\varepsilon)\sqrt{\varepsilon}d\varepsilon$.

Further assuming that superelastic collisions between electrons and atoms, as well as excitation from low to high atomic states, are negligible, from the Boltzmann equation one obtains [43,48]

$$-\frac{2e}{3m_e}\frac{d}{d\varepsilon}\left(\frac{\varepsilon^{3/2}}{\nu_m(\varepsilon)}E_{\mathrm{eff}}^2(\varepsilon)\frac{dF_0}{d\varepsilon}\right) = S_{ea}(F_0) + S_{ee}(F_0) + S_{ed}(F_0), \tag{6}$$

where $E_{\mathrm{eff}} = E_p\nu_m(\varepsilon)/[2(\nu_m^2(\varepsilon)+\omega^2)]^{1/2}$. Here $S_{ea}(F_0)$, $S_{ed}(F_0)$, $S_{ee}(F_0)$ describe the electron-atom, electron-dust, and electron-electron collisions, respectively.

The electron-atom collision term $S_{ea}(F_0)$ has several components. The contribution of elastic collisions is

$$S_{ea}^e(F_0) = \frac{d}{d\varepsilon}\left[\frac{2m_e}{m_i}\varepsilon^{3/2}\nu_m(\varepsilon)\left(F_0 + T_g\frac{dF_0}{d\varepsilon}\right)\right], \tag{7}$$

where $T_g = 0.026$ eV ($\sim$300 K) is the neutral gas temperature. Collision-induced atomic excitations are represented by

$$S_{ea}^{\mathrm{exc}}(F_0) = \sum_k [\nu_{ea}^k(\varepsilon + V_k)F_0(\varepsilon + V_k)(\varepsilon + V_k)^{1/2} - \nu_{ea}^k(\varepsilon)F_0(\varepsilon)\varepsilon^{1/2}], \tag{8}$$

where ν_{ea}^k is the collision frequency of the kth inelastic process with a threshold energy V_k. Ionization is treated as a normal excitation process [49].

Electron-dust interaction includes scattering of the electrons from the shielding potential around the dust, as well as electron loss due to their deposition on the dust grains. The electron-dust collision term can be modeled by [50]

$$S_{ed}(F_0) = \frac{d}{d\varepsilon}\left[\frac{2m_e}{m_d}\varepsilon^{3/2}\nu_{ed}^e\left(F_0 + T_d\frac{dF_0}{d\varepsilon}\right)\right] - \nu_{ed}^c F_0\varepsilon^{1/2}, \tag{9}$$

where $\nu_{ed}^e(\varepsilon)$ and $\nu_{ed}^c(\varepsilon)$ are the momentum transfer and the electron absorption frequencies of electron-dust collisions, respectively, and m_d and T_d are the mass and temperature of the dusts. We shall set $T_d = 0.026$ eV, $m_d = \frac{4}{3}\rho_d\pi a_d^3$, where $\rho_d = 2$ g/cm^3 is the grain material density [1].

The electron-electron collision term $S_{ee}(F_0)$ is given by

$$S_{ee}(F_0) = \frac{d}{d\varepsilon}\left[2\varepsilon^{3/2}\nu_{ee}\left(F_0 G + H\frac{dF_0}{d\varepsilon}\right)\right], \tag{10}$$

with

$$H(\varepsilon) = \frac{2}{3}\left(\int_0^\varepsilon \varepsilon^{3/2}F_0(\varepsilon)d\varepsilon + \varepsilon^{3/2}\int_\varepsilon^\infty F_0(\varepsilon)d\varepsilon\right),$$

and $G(\varepsilon) = \int_0^\varepsilon \varepsilon^{1/2}F_0(\varepsilon)d\varepsilon$, where $\nu_{ee}(\varepsilon) = 4\pi(e^2/m_e)^2 n_e \ln\Lambda/v^3$, $\ln\Lambda$ is the Coulomb logarithm [48], and $T_e = (2/3)\int_0^\infty F_0(\varepsilon)\varepsilon^{3/2}d\varepsilon$ is the electron temperature.

For a given EDF $F_0(\varepsilon)$, the electron current collected by a dust particle in the OML approximation is [51]

$$I_e = -\pi a_d^2 e n_e \int_{-\phi_s}^\infty \left(1 + \frac{\phi_s}{\varepsilon}\right)\sqrt{\frac{2e\varepsilon}{m_e}}F_0(\varepsilon)\sqrt{\varepsilon}d\varepsilon. \tag{11}$$

The ion current on a dust grain is Ref. [52] $I_i = \pi a_d^2 e n_i\sqrt{2eE_0/m_i}(1-\phi_s/E_0)$, where the dust surface potential ϕ_s is related to the dust charge eZ_d by $\phi_s = eZ_d/a_d$. The model assumes that the electron and ion grain currents balance, or

$$I_e + I_i = 0, \tag{12}$$

and that the quasineutrality condition

$$n_e + n_d|Z_d| = n_i \tag{13}$$

is satisfied.

C. Collision cross sections

The electron-neutral and electron-dust collision frequencies appearing in Sec. II B can be obtained by multiplying the electron-neutral and electron-dust cross sections by $n_g\sqrt{2e\varepsilon/m_e}$, where n_g is Ar atom density, and $n_d\sqrt{2e\varepsilon/m_e}$, respectively. We shall consider the same set of cross sections for electron-neutral collisions as in Ref. [53] (see Fig. 1 there). From Ref. [54] we obtain the electron-neutral momentum-transfer cross section σ_m, which agrees well with that obtained experimentally by Ramsauer and Kollath [55] and the one given by O'Malley [56]. The cross section takes into account the characteristic Ramsauer-Townsend drop in σ_m in the low-energy regime. We also use the Ar ionization cross section taken from the experiments of Rapp and Englander-Golden [57]. For describing the excitation processes in the dusty Ar plasma we consider the 4*s*

($^3P_0, ^3P_2, ^1P_1, ^3P_1$), $4p$, and $5s$ excitations. Their cross sections from Refs. [53,58] are in good agreement with that obtained experimentally by Chutjian and Cartwright [59], Borst [60], and McConkey and Donaldson [61].

For the electron-dust interaction potential (1), the electron-dust momentum transfer cross-section can be written as [50]

$$\sigma_{ed}^{e}(\varepsilon) = \pi a_d^2(-\phi_s/\varepsilon)^2 e^{2a_d/\lambda_D} \ln \Lambda, \tag{14}$$

where $\Lambda \simeq -\lambda_D T_e/a_d\phi_s$. In the OML approximation, the cross section of electron collection by a dust grain is $\sigma_{ed}^{c}(\varepsilon) = \pi a_d^2(1+\phi_s/\varepsilon)$ for $\varepsilon \geqslant -\phi_s$ and 0 for $\varepsilon < -\phi_s$.

D. Particle and power balance

To obtain $n_e(\mathbf{r})$ in (5), or the averaged electron density, it is necessary to consider the overall particle and power balance in the discharge. The balance equation for the ions (here Ar^+) can be written as

$$K_{iz} n_e n_g V - K_{id} n_d n_i V_d - n_{is} u_{Bi} S = 0, \tag{15}$$

where u_{Bi} is the velocity of the ion/electron ambipolar flow at the bulk plasma-sheath interface, V and V_d are the total plasma volume and the volume of the dusty plasma, respectively, S is the surface area of the chamber wall, K_{id} is the rate coefficient for ion-dust collisions ($K_{id} n_i = I_i/e$), $K_{iz} = \int \nu_{ea}^{i}(\varepsilon) F_0(\varepsilon) \sqrt{\varepsilon} d\varepsilon / n_g$ is the ionization rate coefficient, and n_{is} is the ion density at the bulk plasma-sheath boundary. For a stable sheath, the plasma flow u_{Bi} is near the Bohm speed [3,62]. For the Maxwellian EDF [$F_0^{\max} = (2/\sqrt{\pi}) T_e^{-3/2} \exp(-\varepsilon/T_e)$], the Bohm speed is $\sqrt{eT_e/m_i}$ [3,63]. For non-Maxwellian EDF, the expression for the ion drift velocity at plasma-sheath interface is given by Ref. [64] $u_{Bi} \approx \sqrt{(2e/m_i)} (\int F_0(\varepsilon) \varepsilon^{-1/2} d\varepsilon)^{-1/2}$.

As mentioned in Sec. II A, a near-wall region of thickness l (for definitiveness we set $l = 0.5$ cm in our calculations) is free from dust grains. Thus, the ions and electrons in these regions behave as in the pristine plasma. The boundary ion density is $n_{is} = n_{eb} \cos(\sqrt{K_{iz} n_g / D_s} l)$, where n_{eb} is electron (or ion) density at a distance l from the boundary. Here, $D_s = D_a/(1 + 2K_{iz} n_g/\nu_{in})$ is an effective diffusion coefficient [53,65], where $D_a = (D_e \mu_i + D_i \mu_e)/(\mu_i + \mu_e)$, $D_i = eE_0/m_i \nu_{in}$, $\mu_i = e/m_i \nu_{in}$,

$$D_e = \frac{2e}{3m_e} \int \frac{\varepsilon^{3/2}}{\nu_m(\varepsilon)} F_0(\varepsilon) d\varepsilon,$$

$$\mu_e = -\frac{2e}{3m_e} \int \frac{\varepsilon^{3/2}}{\nu_m(\varepsilon)} \frac{dF_0(\varepsilon)}{d\varepsilon} d\varepsilon,$$

and ν_{in} is the ion-neutral collision frequency. We note that D_a is the well-known ambipolar diffusion coefficient, D_e and D_i are the electron and ion diffusion coefficients, μ_e and μ_i are the electron/ion mobilities, respectively. Since a dusty plasma is similar to an electronegative discharge, the electron density in the dust-containing region is practically space independent [39], so that $n_{eb} \sim n_e$.

Power balance in the discharge can be described by

$$P_{\text{in}} = P_{ea} + P_w + P_{\text{dust}}, \tag{16}$$

where P_{in} is the total power absorbed by the discharge (in our model P_{in} is an input parameter), P_{ea} is the energy loss via electron-neutral collisions, and P_w and P_{dust} is the power loss in the form of kinetic energy loss through collisions of the plasma species with the walls and dusts, respectively. The power loss via electron-neutral collisions is [35]

$$P_{ea} = e n_e V \left(K_{iz} n_g V_i + \sum_{k=1}^{N_{\text{exc}}} n_g K_{\text{exc}}^{k} V_k + \frac{2m_e}{m_i} \int_0^{\infty} \nu_m(\varepsilon) F_0(\varepsilon) \varepsilon^{3/2} \, d\varepsilon \right), \tag{17}$$

where $K_{\text{exc}}^{k} = \int \nu_{ea}^{k}(\varepsilon) F_0(\varepsilon) \sqrt{\varepsilon} d\varepsilon / n_g$ is the excitation rate coefficient of the kth inelastic process. N_{exc} is the number of excitation processes. The last term in (17) is the energy loss due to electron-neutral elastic scattering.

The power loss at the wall is $P_w = e n_{is} u_{Bi} S(\varepsilon_e + \varepsilon_i)$, where ε_e and ε_i are the mean electron and ion kinetic energies loss (per electron and ion) at the wall, respectively. The mean kinetic energy loss per lost electron is given by the ratio of the average energy flux to the electron flux [66,3]. For an arbitrary electron distribution function F_0 the average kinetic energy per electron lost is given by

$$\varepsilon_e = \frac{\int \varepsilon^2 F_0(\varepsilon) d\varepsilon}{\int \varepsilon F_0(\varepsilon) d\varepsilon},$$

so that for a Maxwellian EDF the mean electron energy loss per lost electron is $\varepsilon_e = 2T_e$. On the other hand, the mean kinetic energy loss per lost ion is the sum of the ion energy entering the sheath and the energy gained by the ion as it traverses the sheath, or $\varepsilon_i = m_i u_{Bi}^2/2e - \Phi_w$, where Φ_w is the (negative) wall potential with respect to the sheath-bulk plasma edge.

To determine the potential Φ_w, we equate the ion flux [3] $\Gamma_i = n_{is} u_{Bi}$, assumed to be constant across the thin sheath, to the electron flux at the wall,

$$\Gamma_e = \frac{1}{4} n_{is} \langle u_e \rangle \exp\left(\frac{\Phi_w}{T_e} \right),$$

where $\langle u_e \rangle = \int \sqrt{2e\varepsilon/m_e} F_0(\varepsilon) \sqrt{\varepsilon} d\varepsilon$ is the mean electron speed, and the electrons are near equilibrium. Since $\Gamma_i = \Gamma_e$, we obtain $\Phi_w = T_e \ln(4u_{Bi}/\langle u_e \rangle)$ for the wall potential. For Maxwellian EDF, we have $m_i u_{Bi}^2/2 = eT_e/2$ and $\Phi_w \sim -4.7 T_e$. Thus, the ions bombard the wall with an energy $\varepsilon_i \sim 5.2 T_e$ [3].

Electrons with energy less than $-\phi_s$ will reflect elastically from a dust grain and re-enter the plasma without altering their energy. An electron with energy higher than $-\phi_s$ will transit through the grain sheath and deposit on the grain surface, together with the leftover energy. The energy lost in the sheath goes into the maintenance of the potential drop in the sheath, and is in turn transferred to the grain by the positive ions accelerated by the sheath potential.

The heat flux associated with the electron current on a dust grain Eq. (11) is

$$q_{ed} = \pi a_d^2 n_e \int_{-\phi_s}^{\infty} \left(1 + \frac{\phi_s}{\varepsilon}\right) \sqrt{\frac{2e\varepsilon}{m_e}} F_0 \varepsilon^{3/2}\, d\varepsilon, \qquad (18)$$

so that the power loss to the dust grains in the plasma volume due to the electron heat flux is

$$P_{\text{dust}} = e q_{ed} n_d V_d. \qquad (19)$$

An ion entering the grain sheath has average energy E_0, which is much smaller than that of the electrons. Thus, P_{dust} as given by Eq. (19) should be a good approximation for the total power lost by the plasma particles to the dust grains.

III. NUMERICAL RESULTS

Equations. (6), (12), (13), (15), and (16) are solved numerically. We are interested in the effects of dust size a_d and density n_d, as well as external parameters such as the input power P_{in} and neutral gas pressure p_0, on the EDF F_0, the electron and ion densities, the electric field E_p sustaining the plasma, and the dust charge eZ_d. The calculations are for conditions typical in ICPs [30], microwave plasmas [27], and the dust growth experiments [1].

A. Effect of dust density

In Fig. 1(a), the EDFs in a pristine and a dusty plasma are presented. The latter is obtained self-consistently from Eqs. (6), (12), (13), (15), and (16). For the pristine case the EDF is calculated from Eqs. (6), (15), and (16) by omitting the dust related terms. We see that there are significant differences in the EDFs. In the low-energy and high-energy regimes the number of electrons in the dusty plasma is higher than that in the pristine one, but the opposite occurs in the mid-energy regime. This difference is due to electron-dust collisions [67].

Note, that in the pristine plasma the EDF is close to Druyvesteyn distribution [68], which because of nonelastic electron-neutral collisions has more electrons at average energy and fewer electrons at high energy than the Maxwellian distribution. The Druyvesteyn distribution has often been observed in dc as well as 13.56 MHz rf discharges at low electron densities ($n_e \leqslant 10^{11}$ cm^{-3} at 100 mTorr) and relatively high electron-neutral collision rates ($\nu_m > \omega$) [69].

In Fig. 1(b) the effect of dust density on the EDF is shown. One can see that increase of n_d is accompanied by increase of electrons in the low-energy ($\varepsilon < 2.5$ eV) as well as the high-energy ($\varepsilon \geqslant 13$ eV) regimes, but a decrease in the midenergy $\varepsilon = 4-10$ eV regime. This behavior can be attributed to momentum transfer via electron-dust collisions [67]. Indeed, since $\nu_{ed}^e \sim n_d$, the electron-dust momentum transfer frequency ν_{ed}^e increases with n_d. The relative number of low-energy electrons in turn increases. The effect is similar to that of electron-electron collisions on the EDF: increase of n_e leads to increase of ν_{ee}, and the distribution evolves towards Maxwellian [63]. The decrease of the EDF in the range 4–10 and the increase in the low-energy range ($\varepsilon < 2.5$ eV) can also be attributed to the Maxwellization, or randomization, of the EDF via electron-dust collisions. This Maxwellization of the EDF with increasing dust density also changes the electron temperature. In fact, we have $T_e = 4.3$, 4.16, and 4.14 eV for $n_d = 10^6$, 2×10^7, and 5×10^7 cm^{-3}, respectively.

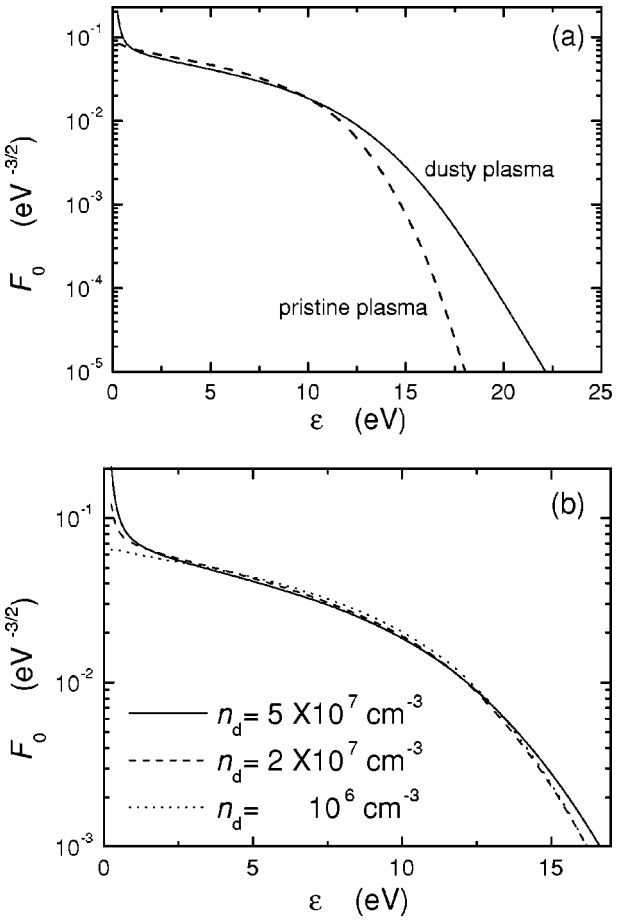

FIG. 1. (a) The EDFs in pristine argon plasma and dust-containing argon discharge at $f_E = 13.56$ MHz, $p_0 = 100$ mTorr, $P_{\text{in}} = 100$ W, $R = L = 10$ cm, $a_d = 100$ nm, and $n_d = 5\times10^7$ cm^{-3}. (b) The EDFs in a dust-containing argon discharge for different dust densities, $n_d = 10^6$, 2×10^7, and 5×10^7 cm^{-3}. The other parameters are the same as in (a).

The increase of electrons in the tail of the EDF is caused by an increase (with n_d) of the electric field E_p sustaining the plasma. We have $E_p = 335$, 352, and 437 V/m for $n_d = 10^6, 2\times10^7$, and 5×10^7 cm^{-3}, respectively. E_p increases self-consistently because with an increase of n_d, the number of electrons and ions lost to the dusts (governed by $K_{id} n_d n_i V_d$) also increases [see Fig. 2(a)], so that the total ionization (given by $K_{iz} n_e n_g V$) in the plasma volume must also increase in order to sustain the balance between the generation and recombination (on the dust grains and wall) of the plasma particles. It is of interest to note that plasma particle loss at the discharge wall decreases as n_d increases, and at high n_d ($\sim 5\times10^7$ cm^{-3}) it is even negligible compared to that to the dusts [see Fig. 2(a)]. Since $n_{is} \sim \cos(l\sqrt{K_{iz} n_g / D_s})$, the decrease of total ion flux ($n_{is} u_{Bi} S$) at the wall can be attributed to a decrease of the boundary ion density n_{is} with n_d. The latter decrease is due to enhanced

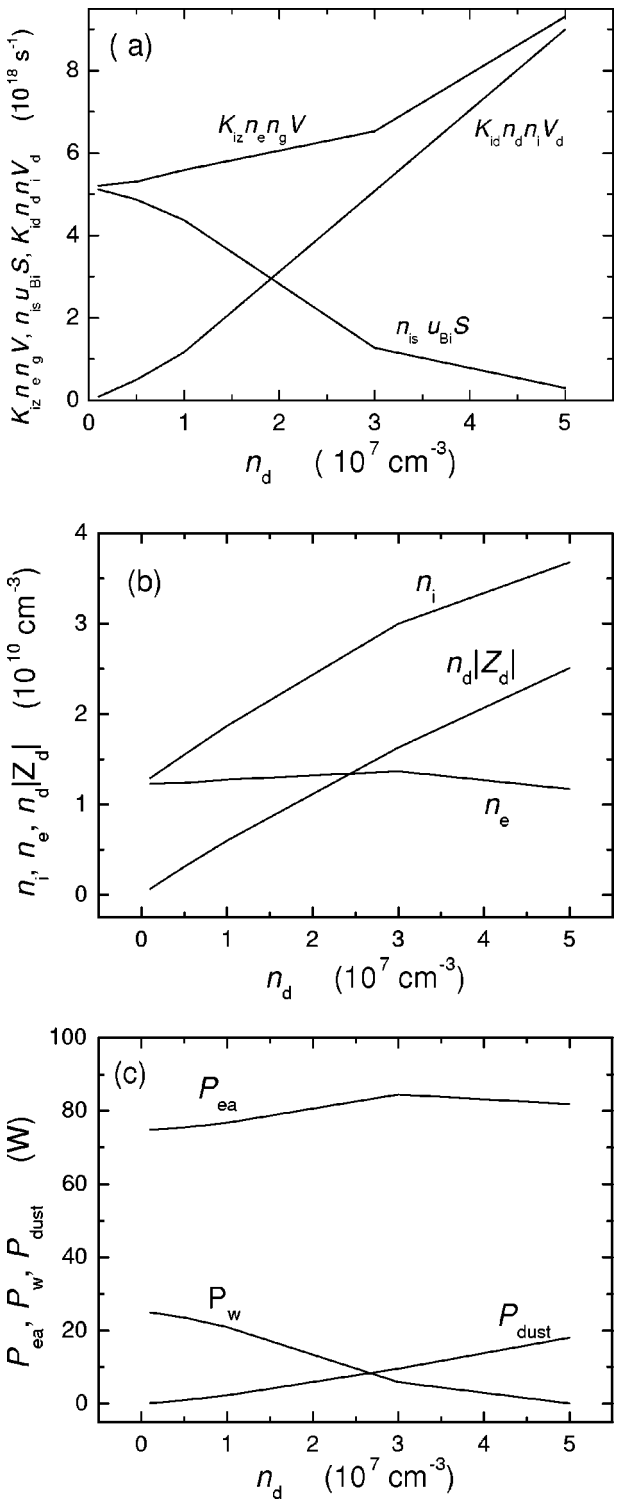

FIG. 2. (a) The rate ($K_{iz}n_e n_g V$) of ion generation in the discharge. The rate of ion loss ($n_{is}u_{Bi}S$) to the discharge wall. The rate ($K_{id}n_d n_i V_d$) of ion loss to the dust grains. (b) Electron and ion densities, and $|n_d Z_d|$. (c) P_{ea}, P_w, and $P_{\rm dust}$ as a function of the dust density n_d. The other parameters are the same as in Fig. 1.

ionization [or $K_{iz}n_g$, see Fig. 2(a)] with increasing n_d.

With increase of n_d the total dust surface collecting electrons and ions is enhanced. Therefore the dust charge $n_d|Z_d|$ per unit plasma volume also increases, as shown in Fig. 2(b). To maintain plasma quasineutrality, the ion density rises with n_d and the electron density decreases slightly [see Fig. 2(c)].

Overall power balance in the discharge also depends on the dust density. The power deposited on the dust grains increases with the total dust surface area in the plasma. The power loss at the wall decreases because n_{is} decreases with n_d increase [see Fig. 2(c)]. At low dust densities about 20% of the power absorbed in the discharge is carried by the electrons and ions to discharge wall [Fig. 2(c)]. At high dust densities the energy loss to the wall is negligible in comparison to that via electron-neutral and electron-dust collisions. In fact, the energy loss to the dust grains is quite high ($\sim 0.2P_{\rm in}$) at high dust densities. Energy absorption by dust grains may lead to heating/excitation of the latter [1,22].

B. Effect of dust size

The effect of dust size on the discharge properties is somewhat similar to that of the dust density. In particular, with increase of a_d the electron-dust collision frequency is enhanced. Comparing the EDFs for $a_d = 50$ nm and $a_d = 150$ nm in Fig. 3(a), one can see that the number of electrons in the low-energy regime ($\varepsilon < 2.5$ eV) is increased while that in the 3–10 eV regime is decreased. The increase of electron and ion loss to the grains is balanced by enhanced ionization from the increase of E_p. For example, we find $E_p = 365$, 521, and 821 V/m for $a_d = 100$, 150, and 200 nm, respectively. The rise of the rf electric field is accompanied by an increase of high-energy electrons in the tail of the EDF. As expected, for larger dusts, an increase of the high-energy electrons is accompanied by a decrease of electrons with $\varepsilon < 10$ eV [see Fig. 3(a) for $a_d = 150$ and 200 nm]. This Maxwellization of the EDF causes T_e to decrease with a_d increase at small dust sizes and/or densities. For large dust size and/or density, because of the high electric field needed to sustain the plasma, one finds that T_e increases with a_d. In fact, $T_e = 4.28$, 4.1, 4.24, and 4.66 eV for $a_d = 50$, 100, 150, and 200 nm, respectively.

Analogously to increasing n_d, increasing the total grain surface area collecting electrons and ions leads to increase of the grain charge density $n_d|Z_d|$. The ion density n_i increases for $a_d \leqslant 125$ nm and decreases for larger a_d. The electron density is practically constant at $a_d \leqslant 100$ nm but decreases for higher dust radii [see Fig. 3(b)]. The decrease of n_i and n_e with a_d increase is due to intensification of electron and ion collection by the dusty grains. The power absorbed in electron-atom collisions increases slightly with a_d [Fig. 3(c)] for $a_d \leqslant 100$ nm because of the increase of high-energy electrons [Fig. 3(a)] at practically constant n_e [see Fig. 3(b)]. At larger dust radii it decreases because of the decrease in n_e. Furthermore, with increase of the dust size, $P_{\rm dust}$ increases and P_w decreases.

C. Effect of pressure

Similar to the pristine case, in a dusty plasma the electron and ion mean free paths increase as the pressure decreases. As a result, diffusion loss of the plasma particles to the wall is enhanced. To compensate for this loss, ionization in the

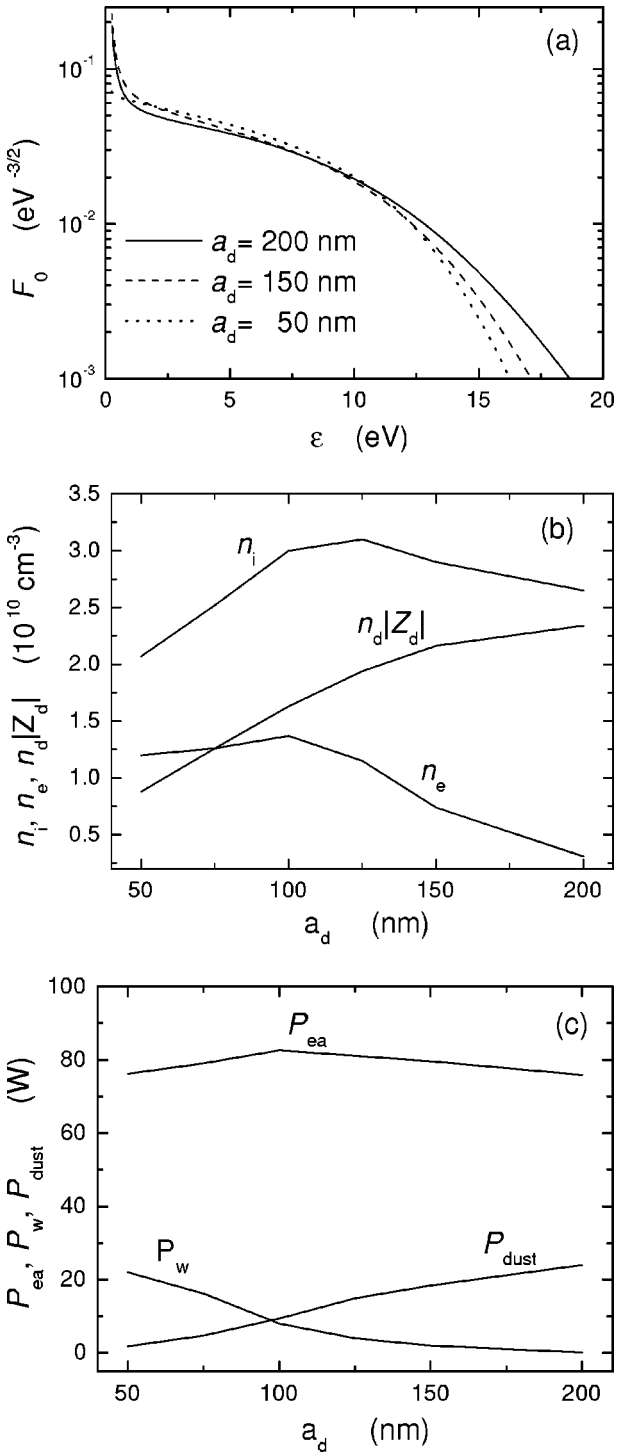

FIG. 3. The EDFs (a) for different dust radii, a_d=50, 150, and 200 nm at $n_d=3\times10^7$ cm^{-3}. (b) Electron and ion densities, and $|n_dZ_d|$. (c) P_{ea}, P_w, and P_{dust} as a function of the dust radius a_d. The other conditions are the same as in Fig. 1.

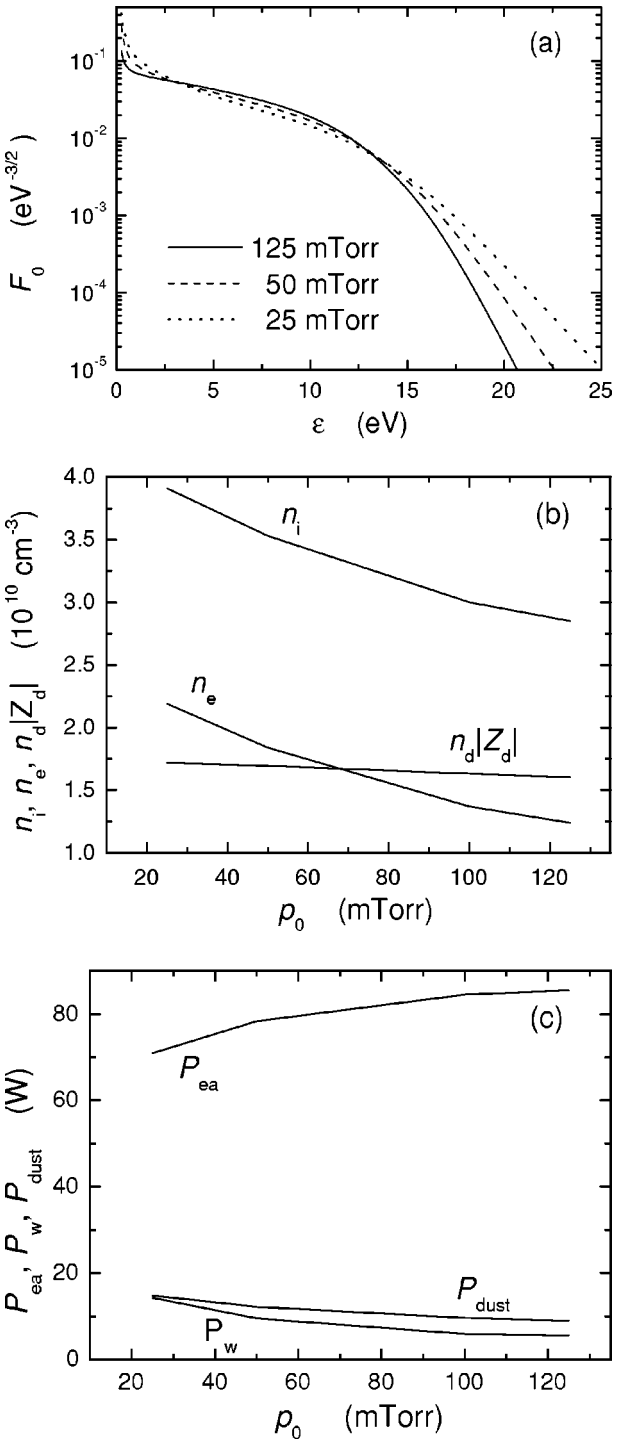

FIG. 4. The EDFs (a) at different neutral gas pressures, p_0=25, 50, and 125 mTorr at a_d=100 nm and $n_d=3\times10^7$ cm^{-3}. Electron and ion densities, and $|n_dZ_d|$ in (b); and P_{ea}, P_w, P_{dust} in (c) in dependence on gas pressure p_0. The other conditions are the same as in Fig. 3.

plasma volume increases via increase of the high energy electrons in the tail of the EDF [see Fig. 4(a)]. However, the electron, ion, and dust-charge densities still decrease [see Fig. 4(b)]. With pressure rise, the number of low energy electrons ($\varepsilon<2.5$ eV) decreases and electrons in the 5–12 eV range increases [Fig. 4(a)]. This EDF behavior in the low-energy range may be associated with electron-electron collisions that Maxwellizes the EDF. The p_0 dependence of the EDF affects T_e, which increases slowly with p_0. We find T_e=3.68, 3.92, and 4.11 eV for p_0=25, 50, and 125 mTorr, respectively.

Neutral gas pressure can also affect the power balance. Figure 4(c) shows the p_0 dependence of the power loss P_{ea} via electron-neutral collisions, the power P_{dust} absorbed by the dust grains, and the power loss P_w at the discharge wall. One can see that the neutral gas density, thus also P_{ea}, increases with p_0. The power loss to the dusts and wall decreases with pressure, as can be attributed to the decrease in the plasma particle densities, especially the number of the high energy electrons.

D. Effect of input power

In Fig. 5(a) the EDFs for different input powers P_{in} are shown. One can see that the number of electrons in the high-energy tail of the EDF increases as power decreases. This behavior can be attributed to the enhanced effect of the dusts on the internal discharge parameters at low input powers. Since with decrease of P_{in} at fixed dust density the electron and ion densities decrease [Fig. 5(b)], the number of dust grains per electron increases. Therefore, the relative electron loss on the dust grains increases as P_{in} decreases. To compensate this additional loss, ionization in the discharge is increased via an enhancement of the high-energy tail of the EDF, and thus also T_e. For example, one finds T_e=4.21, 4.09, 3.87, and 3.8 eV at P_{in}=50, 100, 200, and 400 W, respectively. Consistent with the increase of the number of high-energy electrons, the electric field intensity E_p also increases with the power drop. We found that E_p=392, 365, 311, and 295 V/m at P_{in}=50, 100, 200, and 400 W, respectively. Figure 5(b) also shows that the dusty charge density $n_d|Z_d|$ increases only slightly with P_{in}.

It should be pointed out that for pristine plasmas, T_e also decreases as the input power increases. When the input power is low, electron-electron collisions are rare, and the electron EDF in typical rf discharges is usually Druyvesteyn type. However, when P_{in} increases the electron density also increases, and the enhanced electron-electron collisions tend to Maxwellize the EDF [70]. In general, the T_e corresponding to a Druyvesteyn type EDF is higher than that for the corresponding Maxwellian EDF [66].

For a pristine plasma at external conditions corresponding to Fig. 5(a), one finds that T_e=3.92, 3.86, 3.76, and 3.55 eV, and E_p=182, 176, 165, and 148 V/m for P_{in}=50, 100, 200, and 400 W, respectively. We see that in the presence of dusts, E_p is higher than that in the pristine plasma. This occurs because the electron loss in dust containing plasmas is higher. Indeed, as can be seen in Fig. 1(a), the number of high-energy electrons and E_p are both higher than that in the pristine case. Electron-impact ionization is thereby also enhanced. It should also be noted that when P_{in} varies from 50 to 200 W, the changes in T_e and E_p are much more pronounced than that in the pristine plasma. This behavior can be attributed to the enhanced role of electron-dust collisions at low input powers.

Figure 5(c) shows that the ratios P_{ea}/P_{in} and $P_{\text{dust}}/P_{\text{in}}$ both decrease with power. The former is associated with a decrease of high energy electrons in the EDF, leading to a decrease (with P_{in}) of the energy loss in electron-neutral collisions. On the other hand, the decrease of $P_{\text{dust}}/P_{\text{in}}$ is associated with a decrease of the number n_d/n_e of dust grains per electron at fixed dust density. Because P_{ea}/P_{in} and $P_{\text{dust}}/P_{\text{in}}$ both decrease the energy absorption by the discharge wall is enhanced.

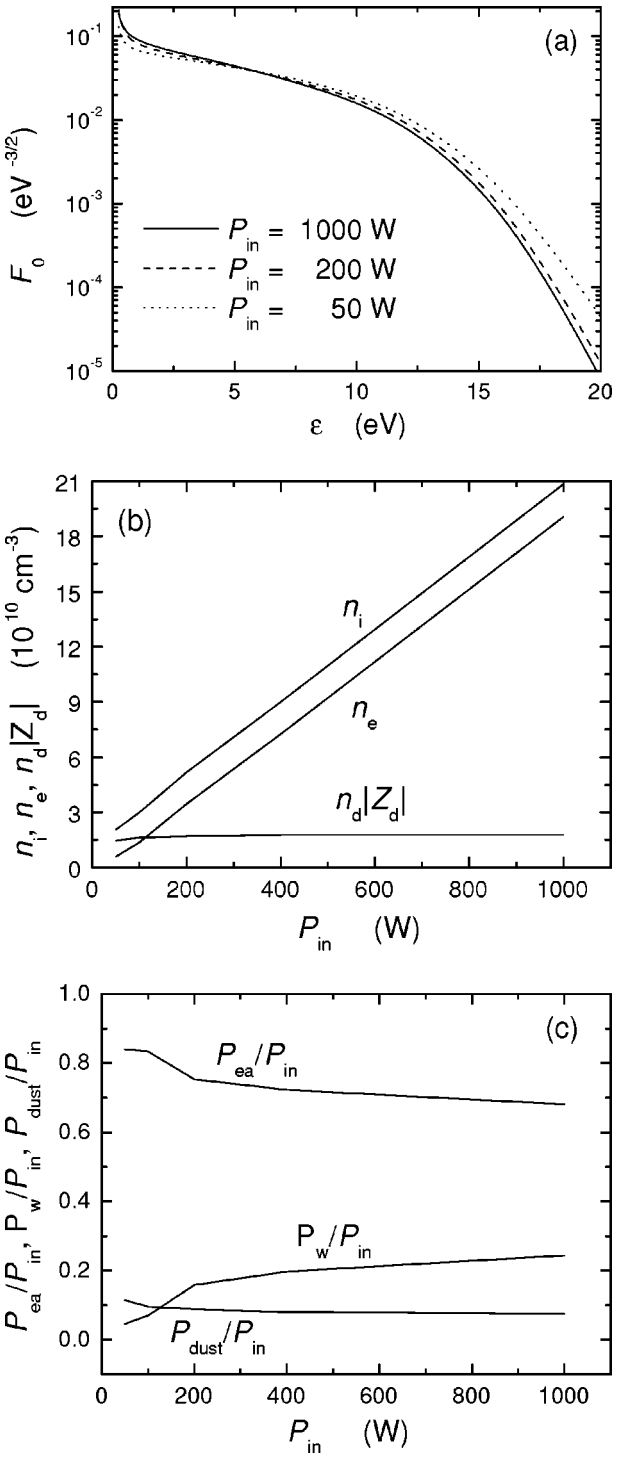

FIG. 5. (a) The EDFs for different input powers, P_{in}=50, 200, and 1000 W at p_0=100 mTorr. (b) Electron and ion densities, and $n_d|Z_d|$. (c) P_{ea}/P_{in}, P_w/P_{in}, $P_{\text{dust}}/P_{\text{in}}$ versus P_{in}. The other parameters are the same as in Fig. 4.

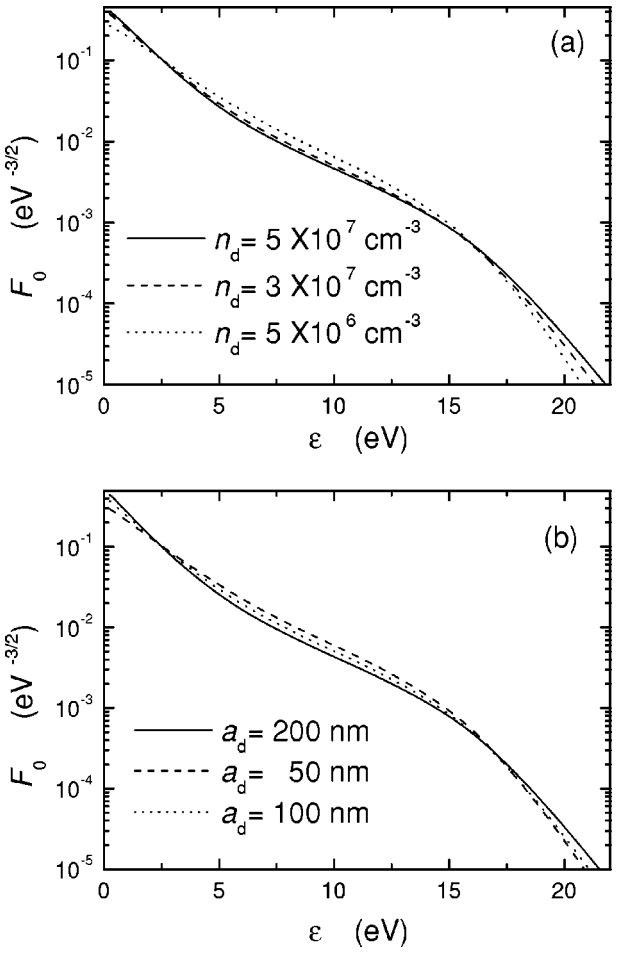

FIG. 6. (a) The EDFs for different dust densities, $n_d=5\times10^6$, 3×10^7, and 5×10^7 cm^{-3} at $a_d=100$ nm . (b) The same as in (a) for different dust radii, $a_d=50$, 100, and 200 nm at $n_d=10^7$ cm^{-3}. Here $R=L=10$ cm, $p_0=100$ mTorr, $P_{\text{in}}=1$ kW, and the generator frequency $f_E=2.45$ GHz.

IV. MICROWAVE DISCHARGE

We now consider dusty microwave discharges driven at $f_E=2.45$ GHz. The calculated EDFs at $n_d=5\times10^6$, 3×10^7, and 5×10^7 cm^{-3} are shown in Fig. 6(a). In contrast to that of the ICPs driven at lower frequencies, the EDFs in the dusty microwave plasma as well as in a high-frequency pristine discharge [63] are close to Maxwellian. Dust grains only slightly affect the profile of the EDF. With increase of dust density the number of high energy electrons in the tail of the EDF increases, leading to increased ionization which in turn balances the enhanced electron loss on the dust grains. This self-consistent process is similar to that occurring in rf ICPs discussed in Sec. III A. The enhancement of the EDF tail is due to an increase of E_p: we have $E_p=6245$, 7399, and 8239 V/m for $n_d=5\times10^6$, 3×10^7, and 5×10^7 cm^{-3}, respectively. Like in rf driven plasmas, low-energy ($\varepsilon<2.5$ eV) electrons increase with n_d, but the number of electrons in the 5 eV $<\varepsilon<15$ eV range is reduced. As a result, as n_d increases, T_e decreases. For example, one finds that $T_e=2.55$, 2.24, and 2.14 eV for $n_d=5\times10^6$, 3×10^7, and 5×10^7 cm^{-3}, respectively.

Because of the increase of electrons on the dust grains, the (negative) dust charge per unit plasma volume increases with n_d. One finds $n_d|Z_d|=2.56\times10^9$, 1.44×10^{10}, and 2.35×10^{10} cm^{-3} for $n_d=5\times10^6$, 3×10^7, and 5×10^7 cm^{-3}, respectively. Also similar to an rf discharge, the power loss to the dust grains increases and that to the wall decreases with n_d. For example, one has $P_{\text{dust}}=14.1$, 83, and 128 W, $P_w=201$, 120, and 74 W for $n_d=5\times10^6$, 3×10^7, and 5×10^7 cm^{-3}, respectively.

The effect of dust radius on the EDF is also similar to that of the dust density. In Fig. 6(b) the EDFs for different dust radii are shown. In particular, with increase of a_d, the number of electrons with $\varepsilon\leqslant2.5$ eV and $\varepsilon\geqslant18$ eV in the EDF are enhanced, but in the mid-energy range (5 eV$\leqslant\varepsilon\leqslant16$ eV) it is reduced.

V. DISCUSSION

In this section we discuss the results in a more unified manner. First, the characteristics of dusty ICPs and microwave plasmas can be managed by controlling certain external parameters. In particular, by increasing the input power one can raise the electron and ion densities as well as the averaged dust charge. The electron temperature then drops slightly because of a decrease of the relative dust density with respect to the electron and ion densities. On the other hand, the electron and ion densities, together with the averaged dust charge, decrease with the plasma pressure. This can be attributed to a decrease of high energy electrons, associated with a decrease of the ionization level with p_0.

The plasma properties also depend strongly on the dust density or size. With increase of the former, the EDF is enhanced in the low-energy regime and decreases in the midenergy regime, accompanied by decrease of T_e. Our results show that when n_d or a_d increase, the electric field sustaining the plasma also increases. This behavior is in a good agreement with the results of earlier studies [50,67]. In particular, using a hybrid fluid model with Monte Carlo and molecular dynamics simulations McCaugney and Kushner [67] reported that at fixed electric field, T_e decreases with the dust density. Taking into account the diffusion of electrons to the plasma boundaries it was also shown [67] that the electric field sustaining the plasma increases with n_d, which is in a remarkable agreement with the results of Secs. III A and III B. On the other hand, if E_p does not change much (one of the limiting cases in Refs. [67,50]), T_e either decreases or remains fairly constant when n_d or a_d become larger (as demonstrated in Secs. III A, III B, and IV).

We have also shown that with an increase of n_d or a_d, the number of high energy particles in the EDF increases. This agrees well with the experiments of Tachibana *et al.* [71], where the EDFs were measured in a parallel-plate dusty rf argon discharge. In particular, it was found [71] that the number of electrons in the tail of the EDF is higher, and the EDF is closer to the Maxwellian EDF, as compared to the pristine plasma case. This elevated population of higher-energy electrons have also been observed in the dust void experiments [72,73].

In fact, with increase of n_d or a_d the electron loss in the plasma also increases. This loss is compensated by an en-

hancement of the ionization level associated with the increase of the high-energy electrons in the EDF tail. To complete the picture of the dynamic self-consistent process, we note that with increase of n_d or a_d, the dust-charge density also increases. To maintain the overall plasma neutrality the ion density n_i also increases comparing with that at low n_d or a_d. As a result of a balance between ionization and electron loss, the electron density increases slightly at low dust densities ($n_d < 3\times10^7$ cm^{-3}) or dust radii ($a_d < 100$ nm) and decreases at high dust densities or radii. It is of interest to note that the power absorbed by the dust grains can be quite high ($\sim$20% of P_{in}) and can actually exceed that deposited at the wall.

The global model proposed here allows one to predict the averaged plasma parameters, such as the EDF, the electron and ion number densities, the electron temperature, and the dust charge. The study represents a significant improvement on most existing investigations on dusty discharges [22,23], where the Maxwellian energy distribution is invoked. We have also taken into account the detailed power balance in the plasma, including the power loss at the dust grains, electron-neutral collisions, as well as the discharge wall. It should be pointed out that while most earlier theories [1] for dusty discharges can be applied to CCPs at low ($n_i \leqslant 10^9$ cm^{-3}) densities, they are in general not applicable to modern high-density industrial ICPs and microwave plasmas.

In our calculations, the size and density of the dust grains are that typically found in the laboratory experiments on complex plasmas [1]. In reality, they are correlated and should depend on the neutral gas pressure, temperature, as well as the discharge volume. To self-consistently calculate the evolution of the dust size and concentration, a much more detailed formulation including the dust nucleation and agglomeration processes [6,23] is required. However, at present the latter processes are still not yet well understood.

In developing the global model, several simplifying assumptions have been made. We now discuss in more detail their limitations and implications. First, we have assumed that the dust grains are uniformly distributed in the plasma volume. This is close to the typical roughly uniform distribution found in experiments where the dust grains are chemically formed [1,38] or externally injected [74]. In the experiments the electron and ion densities are also nearly uniform [39]. Thus, in calculating the EDF we can neglect the spatial variation of the EDF if the external electric field is uniform. On the other hand, in certain experiments dust grains sometimes accumulate near the boundary [75,76]. In this case the dust density can be nonuniform and can lead to nonuniformity of the electrons and ions [37]. Thus, the electron EDF will also be nonuniform, and the present global model will no longer be appropriate and a model taking into account spatial effects must be introduced.

We have considered steady-state conditions assuming that the dusts are fixed. In many rf argon-silane discharges this may not be the case [1,6]. Nevertheless, the dust growth process is very slow in comparison with the diffusion and collision processes that determine the EDF. For example, approximately 5 seconds are required for growth of the dust size from 50 nm to 60 nm [38]. Thus, dust growth can safely be treated in a quasistationary manner.

Relatively large (exceeding a few tens of nm in radius) dusts have been considered. Such a size falls within the validity of the OML theory [77]. Extension of our study to the nanometer ($\sim$1–10 nm) or lower domains would require substantial upgrading of the existing dust-charging theories to account for the plasma particle trapping by the wall potential as well as other effects.

Finally, we have ignored the reactive chemistries and formation of the dust grains, as well as the possible existence of negatively charged ions. The chemistries are crucial in determining the composition of the complex plasma. The negative ions can significantly affect the EDF since they can take up much of the negative charge in the plasma system. On the other hand, our model can be directly applied to plasmas containing dust grains that are externally injected, as in many laboratory experiments.

VI. CONCLUSION

A model for argon plasmas containing charged dusts has been introduced. The model allows one to find the averaged electron EDF, the electron and ion densities, the electron temperature, as well as the average dust charge. Numerical solutions based on the model demonstrate how a low-pressure diffusion equilibrium of the complex plasma system is self-consistently sustained by plasma particle sources and sinks. The power lost to the dust grains in the complex plasma is compared to that lost to electron-neutral collisions and the wall. Variations of the input power, working gas pressure, dust size, and density result in significant modifications in the electron energy distribution, electron temperature, electron and ion densities, as well as dust charge.

In spite of the many limitations, the model considered here is relatively simple and accounts for the major particle sources and sinks in a typical dusty plasma system. The model describes the effects of the dust grains on the EDF, the electron and ion densities, and the electron temperature. It allows one to analyze power balance in the complex discharge taking into account energy loss to the dust grains. Our model can be easily extended to electronegative reactive dusty plasmas [78,79].

ACKNOWLEDGMENTS

One of the authors (I.D.) was supported by the Humboldt Foundation. This work was partially supported by the Australian Research Council, the University of Sydney, the Agency for Science, Technology and Research, the Lee Kuan Yew Foundation, and NATO.

[1] *Dusty Plasmas: Physics, Chemistry, and Technological Impacts in Plasma Processing*, edited by A. Bouchoule (Wiley, New York, 1999).
[2] S. V. Vladimirov and K. Ostrikov, Phys. Rep. **393**, 175 (2004).
[3] M. A. Lieberman and A. J. Lichtenberg, *Principles of Plasma Discharges and Materials Processing* (Wiley, New York, 1994).
[4] *ULSI Technology*, edited by C. Y. Chang and S. M. Sze (McGraw-Hill, New York, 1996).
[5] M. Chhowalla, K. B. K. Teo, C. Ducati, N. L. Rupesinghe, G. A. J. Amaratunga, A. C. Ferrari, D. Roy, J. Robertson, and W. I. Milne, J. Appl. Phys. **90**, 5308 (2001), and the references therein.
[6] Ch. Hollenstein, Plasma Phys. Controlled Fusion **42**, R93 (2000).
[7] L. Boufendi and A. Bouchoule, Plasma Sources Sci. Technol. **11**, A211 (2002), and the references therein.
[8] M. Meyyappan, L. Delzeit, A. Cassell, and D. Hash, Plasma Sources Sci. Technol. **12**, 205 (2003), and references therein.
[9] K. Ostrikov, Sing. J. Phys. **19**, 1 (2003), and references therein.
[10] I. B. Denysenko, S. Xu, P. P. Rutkevych, J. D. Long, N. A. Azarenkov, and K. Ostrikov, J. Appl. Phys. **95**, 2713 (2004).
[11] Z. L. Tsakadze, K. Ostrikov, J. D. Long, and S. Xu, Diamond Relat. Mater. **13**, 1923 (2004).
[12] M. Takai, T. Nishimoto, M. Kondo, and A. Matsuda, Appl. Phys. Lett. **77**, 2828 (2000).
[13] P. Roca i Cabarrocas, J. Non-Cryst. Solids **266**, 31 (2000).
[14] J. Giapintzakis, J. Androulakis, A. V. Rode, E. G. Gamaly, A. G. Christy, J. G. Fitz Gerald, T. Hyde, R. G. Elliman, and B. Luther-Davies, Annual APS March Meeting 2004, March 22–26, 2004, Montreal, Quebec, Canada, Contrib. A17.005; A. V. Rode, R. G. Elliman, E. G. Gamaly, A. I. Veinger, A. G. Christy, S. T. Hyde, and B. Luther-Davies, Appl. Surf. Sci. **197**, 644 (2002).
[15] I. B. Denysenko, K. Ostrikov, S. Xu, M. Y. Yu, and C. H. Diong, J. Appl. Phys. **94**, 6097 (2003).
[16] M. Goto, H. Toyoda, M. Kitagawa, T. Hirao, and H. Sugai, Jpn. J. Appl. Phys., Part 1 **36**, 3714 (1997).
[17] K. Goshima, H. Toyoda, T. Kojima, M. Nishitani, M. Kitagawa, H. Yamazoe, and H. Sugai, Jpn. J. Appl. Phys., Part 1 **38**, 3655 (1999).
[18] T. Kojima, A. Ohishi, H. Toyoda, M. Goto, M. Nishitani, and H. Sugai, Jpn. J. Appl. Phys., Part 1 **40**, 322 (2001).
[19] K. N. Ostrikov, M. Y. Yu, and H. Sugai, J. Appl. Phys. **86**, 2425 (1999).
[20] K. N. Ostrikov and M. Y. Yu, J. Phys. D **32**, 1650 (1999).
[21] S. V. Vladimirov and N. F. Cramer, Phys. Rev. E **62**, 2754 (2000).
[22] A. A. Fridman, L. Boufendi, T. Hbid, B. V. Potapkin, and A. Bouchoule, J. Appl. Phys. **79**, 1303 (1996).
[23] U. Kortshagen and U. Bhandarkar, Phys. Rev. E **60**, 887 (1999).
[24] V. N. Tsytovich, Phys. Usp. **40**, 53 (1997) [Usp. Fiz. Nauk **167**, 57 (1997)], and the references therein.
[25] V. A. Godyak, B. M. Alexandrovich, and V. I. Kolobov, Phys. Rev. E **64**, 026406 (2001).
[26] S. Xu, K. N. Ostrikov, Y. Li, E. L. Tsakadze, and I. R. Jones, Phys. Plasmas **8**, 2549 (2001).
[27] See, for example, *Microwave Discharges: Fundamentals and Applications, NATO Advanced Studies Institute, Series B: Physics*, Vol. 302, edited by C. M. Ferreira and M. Moisan (Plenum, New York, 1993).
[28] H. M. Wu, B. W. Yu, A. Krishnan, M. Li, Y. Yang, J. P. Yan, and D. P. Yuan, IEEE Trans. Plasma Sci. **25**, 776 (1997).
[29] R. A. Stewart, P. Vitello, D. B. Graves, E. F. Jaeger, and L. A. Berry, Plasma Sources Sci. Technol. **4**, 36 (1995).
[30] I. Denysenko, S. Dudin, A. Zykov, N. Azarenkov, and M. Y. Yu, Phys. Plasmas **9**, 4767 (2002).
[31] V. I. Kolobov and V. A. Godyak, IEEE Trans. Plasma Sci. **23**, 503 (1995).
[32] U. Kortshagen, C. Busch, and L. D. Tsendin, Plasma Sources Sci. Technol. **5**, 1 (1996).
[33] C. K. Birdsall, IEEE Trans. Plasma Sci. **19**, 65 (1991).
[34] D. Vender and R. W. Boswell, IEEE Trans. Plasma Sci. **18**, 725 (1990).
[35] C. Lee and M. A. Lieberman, J. Vac. Sci. Technol. A **13**, 368 (1995).
[36] A. V. Vasenkov and B. D. Shizgal, Phys. Plasmas **9**, 691 (2002); Phys. Rev. E **65**, 046404 (2002).
[37] K. Ostrikov, I. B. Denysenko, S. V. Vladimirov, S. Xu, H. Sugai, and M. Y. Yu, Phys. Rev. E **67**, 056408 (2003).
[38] A. Bouchoule and L. Boufendi, Plasma Sources Sci. Technol. **2**, 204 (1993).
[39] Ph. Belenguer, J. Ph. Blondeau, L. Boufendi, M. Toogood, A. Plain, A. Bouchoule, C. Laure, and J. P. Boeuf, Phys. Rev. A **46**, 7923 (1992).
[40] J. E. Daugherty, R. K. Porteous, M. D. Kilgore, and D. B. Graves, J. Appl. Phys. **72**, 3934 (1992).
[41] R. V. Kennedy and J. E. Allen, J. Plasma Phys. **69**, 485 (2003).
[42] S. Chapman and T. G. Cowling, *Mathematical Theory of Non-Uniform Gases* (Cambridge University Press, Cambridge, 1958).
[43] I. P. Shkarofsky, T. W. Johnston, and M. P. Bachynski, *The Particle Kinetics of Plasma* (Addison-Wesley, Reading, MA, 1966).
[44] U. Kortshagen, Plasma Sources Sci. Technol. **4**, 172 (1995).
[45] R. Winkler, J. Wilhelm, and A. Hess, Ann. Phys. (Leipzig) **42**, 537 (1985).
[46] R. Winkler, M. Capitelli, M. Dilonardo, C. Gorse, and J. Wilhelm, Plasma Chem. Plasma Process. **6**, 437 (1986).
[47] C. M. Ferreira and M. Moisan, Phys. Scr. **38**, 382 (1988).
[48] L. M. Biberman, V. S. Vorobev, and I. T. Yakubov, *Kinetics of Nonequilibrium Low-Temperature Plasma* (Moscow, Nauka, 1982).
[49] C. M. Ferreira and J. Loureiro, Plasma Sources Sci. Technol. **9**, 528 (2000).
[50] D. Wang and J. Q. Dong, J. Appl. Phys. **81**, 38 (1997).
[51] W. Lochte-Holtgreven, *Plasma Diagnostics* (North-Holland, Amsterdam, 1968), p. 675.
[52] H. M. Mott-Smith and I. Langmuir, Phys. Rev. **28**, 727 (1926).
[53] U. Kortshagen, H. Schlüter, and A. Shivarova, J. Phys. D **24**, 1571 (1991).
[54] L. S. Frost and A. V. Phelps, Phys. Rev. **136**, A1538 (1964).
[55] C. Ramsauer and R. Kollath, Ann. Phys. (Leipzig) **12**, 529 (1932).
[56] T. F. O'Malley, Phys. Rev. **130**, 1020 (1963).
[57] D. Rapp and P. Englander-Golden, J. Chem. Phys. **43**, 1464 (1965).

[58] C. M. Ferreira and J. Loureiro, J. Phys. D **16**, 1611 (1983).
[59] A. Chutjian and D. C. Cartwright, Phys. Rev. A **23**, 2178 (1981).
[60] W. L. Borst, Phys. Rev. A **9**, 1195 (1974).
[61] J. W. McConkey and F. G. Donaldson, Can. J. Phys. **51**, 914 (1973).
[62] K. U. Riemann, J. Phys. D **24**, 493 (1991), and the references therein.
[63] V. E. Golant, A. P. Zhilinskii, and I. E. Sakharov, *Fundamentals of Plasma Physics* (Wiley, New York, 1980).
[64] H. Amemiya, J. Phys. Soc. Jpn. **66**, 1335 (1997).
[65] J. H. Ingold, in *Gaseous Electronics*, edited by M. N. Hirsh and H. J. Oskam (Academic, New York, 1978).
[66] J. T. Gudmundsson, Plasma Sources Sci. Technol. **10**, 76 (2001).
[67] M. J. McCaughey and M. J. Kushner, J. Appl. Phys. **69**, 6952 (1991).
[68] M. J. Druyvesteyn and F. M. Penning, Rev. Mod. Phys. **12**, 87 (1940).
[69] V. A. Godyak, R. B. Piejak, and B. M. Alexandrovich, Plasma Sources Sci. Technol. **11**, 525 (2002); Phys. Rev. Lett. **68**, 40 (1992).
[70] M. M. Turner and M. A. Lieberman, Plasma Sources Sci. Technol. **8**, 313 (1999).
[71] K. Tachibana, Y. Hayashi, T. Okuno, and T. Tatsuta, Plasma Sources Sci. Technol. **3**, 314 (1994).
[72] D. Samsonov and J. Goree, Phys. Rev. E **59**, 1047 (1999).
[73] D. Samsonov and J. Goree, IEEE Trans. Plasma Sci. **27**, 76 (1999).
[74] K. Tachibana and Y. Hayashi, Pure Appl. Chem. **68**, 1107 (1996).
[75] A. Garscadden, B. N. Ganguly, P. D. Haaland, and J. Williams, Plasma Sources Sci. Technol. **3**, 239 (1994).
[76] N. Hayashi, Phys. Plasmas **8**, 3051 (2001).
[77] M. S. Barnes, J. H. Keller, J. C. Forster, J. A. O'Neill, and D. K. Coultas, Phys. Rev. Lett. **68**, 313 (1992).
[78] S. Stoykov, C. Eggs, and U. Kortshagen, J. Phys. D **34**, 2160 (2001).
[79] K. Takahashi and K. Tachibana, J. Appl. Phys. **89**, 893 (2001); J. Vac. Sci. Technol. A **19**, 2055 (2001).